*Journal of The Electrochemical Society*, **147** (6) 2061-2069 (2000)
S0013-4651(99)10-069-7 CCC: $7.00 © The Electrochemical Society, Inc.


# Synthesis and Characterization of New $LiNi_{1-y}Mg_yO_2$ Positive Electrode Materials for Lithium-Ion Batteries

**C. Pouillerie,[a,b] L. Croguennec,[a] Ph. Biensan,[b,*] P. Willmann,[c] and C. Delmas[a,*,z]**

[a]*Institut de Chimie de la Matière Condensée de Bordeaux-CNRS and Ecole Nationale Supérieure de Chimie et Physique de Bordeaux, 33608 Pessac Cedex, France*
[b]*SAFT, Direction de la Recherche, 33074 Bordeaux Cedex, France*
[c]*CNES, 31055 Toulouse Cedex, France*

New $LiNi_{1-y}Mg_yO_2$ ($0 \leq y \leq 0.20$) layered oxides were synthesized by a coprecipitation method followed by a high-temperature thermal treatment. Rietveld refinements of their X-ray diffraction patterns showed that they exhibit a quasi-two-dimensional structure, isostructural to $LiNiO_2$, for small substitution amounts ($y \leq 0.10$). For larger amounts ($y = 0.15, 0.20$), the Li/(Ni + Mg) ratio is significantly lower than unity. In all cases, the extra ions located in the inter-slab space for lithium deficiency compensation are preferentially $Mg^{2+}$ ions. A magnetic study confirmed the cationic distributions which result from the size difference between $Ni^{3+}$ and $Mg^{2+}$ ions. An electrochemical study showed reversible behavior for all materials. A high capacity ($\geq$150 Ah $kg^{-1}$) was found for $LiNi_{1-y}Mg_yO_2$ phases ($y \leq 0.02$), which decreased when $y$ increased. The presence of $Mg^{2+}$ cations in the inter-slab space, which cannot be oxidized and have a size close to $Li^+$, prevents the local collapses of the structure which occurs for the $Li_{1-z}Ni_{1+z}O_2$ system; therefore good cycling stability is observed.


Manuscript submitted October 18, 1999; revised manuscript received February 17, 2000.

Since the development of lithium-carbon batteries, $LiNiO_2$ has been considered a promising positive electrode material for rechargeable lithium batteries due to its low cost and high energy density.[1-5] Its structure can be described as a packing of $NiO_2$ slabs between which lithium ions are inserted.[6] It is, however, well known that its true formula is $Li_{1-z}Ni_{1+z}O_2$ with $z$ extra nickel ions located in the lithium site. During the last few years, numerous studies have been devoted to the improvement of the lithium nickelate stoichiometry, which is strongly dependent on its preparation conditions[7-9] and significantly influences the electrochemical properties of the material.[7,9,10] It was recently demonstrated that the loss of reversibility at the first cycle in $Li_xC_6$//$Li_xNi_{1+z}O_2$ cells is strongly related to the oxidation of the extra nickel ions during the first charge, which induces an irreversible shrinkage of the inter-slab space.[10,11]

However, before the advent of possible commercial applications, $LiNiO_2$ still must be optimized due to its thermal instability in organic electrolytes in its charged state, which can result in safety problems.[12-14] Furthermore, the problem of capacity fading observed upon long-term cycling must be overcome.[3] Until now, the origin of this fading has not been understood because neither structural nor textural modification has been detected on electrodes recovered after 1200 cycles at the C rate.[15,16]

Because cationic substitution for nickel appears to be a good method to modify the structural and electrochemical properties of lithium nickelate, increasing activity has been devoted during the past few years to the synthesis and characterization of new substituted $LiNi_{1-y}M_yO_2$ materials (M = Co, [17-21] Al, [13,22-26] Fe, [27-30] Ti, [31,32] Mn, [33-37] Ga, [38] B, [39] Ti and Mg, [40] Ga and Mg, [41]...). For example, structural studies performed on the $LiNi_{1-y}Co_yO_2$ system showed that pure 2D materials are obtained for $y \geq 0.30$, [17,19,20,42] with very good electrochemical properties.[18,42] Ohzuku *et al.* reported that partial aluminum substitution for nickel effectively stabilizes the structure of fully deintercalated phases and therefore improves battery safety.[13,24] Substitution of diamagnetic cations such as $Al^{3+}$ or $Ga^{3+}$ [38] for nickel also prevents electrode overcharge by reducing the amount of lithium ions which can be deintercalated from the $Li_xNi_{1-y}M_yO_2$ active material.

More recently, FMC investigated the properties of novel $LiNi_{1-y}Mg_{y/2}Ti_{y/2}O_2$ compounds ($0 \leq y \leq 0.30$).[40] According to the authors, simultaneous substitution of Mg and Ti for Ni enables one to obtain good cycling stability and safe thermal behavior in the charged state. However, no explanation for these results was proposed. A study of magnesium-substituted lithium cobaltite was recently reported by Tukamoto *et al.*[43] and showed that the conductivity of the $LiCo_{1-y}Mg_yO_2$ phases increases upon substitution due to a mechanism of charge compensation involving the formation of holes in the $t_2$ cobalt band.

Both $LiNi_{0.86}Co_{0.09}Mg_{0.05}O_2$ and $LiNi_{0.91}Co_{0.09}O_2$ materials were recently long-term cycled in SAFT laboratories: 500 cycles at the C rate were achieved at 60°C.[44] The result showed that 0.08 and 0.02% of the reversible capacity were lost per cycle upon cycling for the Co and the MgCo substituted systems, respectively. In the latter case, the suppression of capacity fading was consequently related to partial magnesium substitution for nickel. Therefore, it appeared important to determine the effect of magnesium substitution for nickel on the properties of lithium nickelate.

Novel magnesium-substituted lithium nickelate $LiNi_{1-y}Mg_yO_2$ ($0 \leq y \leq 0.20$) phases were synthesized and characterized from the structural, magnetic and electrochemical points of view. For low magnesium contents, we expected to replace the $Ni^{2+}$ ions present in the $Li_{1-z}Ni_{1+z}O_2$ phases by $Mg^{2+}$ ions. Moreover, good electrochemical properties were expected for the magnesium-substituted materials, because the diamagnetic $Mg^{2+}$ ions do not participate in the redox process, and therefore should not induce shrinkage of the inter-slab space upon lithium deintercalation. In order to achieve better understanding of the effect of magnesium on the structural and electrochemical properties of the $LiNi_{1-y}Mg_yO_2$ phases, the amount of substitution was extended to $y = 0.20$.

## Experimental

The $LiNi_{1-y}Mg_yO_2$ ($0 \leq y \leq 0.40$) materials were synthesized by a coprecipitation method in aqueous solution as described in detail by Caurant *et al.*[45] This synthesis method was chosen because intimate mixing of the various reagents favors higher reactivity and a greater homogeneity of the as-synthesized materials due to a more statistical distribution during thermal treatment.

A 1 M solution of $Ni(NO_3)_2$ and $Mg(NO_3)_2$ was prepared in a $(1-y)/y$ molar ratio with $0 \leq y \leq 0.40$. This solution was added while stirring to a solution of 1 M LiOH and 3 M $NH_4OH$ (Li/(Ni + Mg) = 1.05). An excess of lithium was used in order to compensate for lithium loss during the calcination process and thereby limit any lithium deficiency of the as-synthesized samples. Blue-green coprecipitates were obtained, and the remaining water and ammonia were removed in a rotary evaporator at 70°C under primary vacuum. The resulting products were then dried for 20 h at 110°C in air. The

* Electrochemical Society Active Member.
z E-mail: delmas@icmcb.u-bordeaux.fr

S0013-4651(99)10-069-7 CCC: $7.00 

ground mixtures were heated under a flow of dry oxygen for 5 h at 700°C (for $0 \leq y \leq 0.03$) and at 750°C (for $0.05 \leq y \leq 0.20$) in order to obtain single-phase materials. Several attempts to prepare pure $LiNi_{1-y}Mg_yO_2$ phases (with $y > 0.20$) were made at temperatures between 750 and 850°C.

All samples were characterized by X-ray diffraction (XRD). The XRD patterns were collected using a Siemens D5000 diffractometer equipped with a diffracted-beam monochromator (Cu Kα radiation) at the 10-70° (2θ) for routine characterization. For our structural study (Rietveld refinement), data were collected in the 10-120° (2θ) range in steps of 0.02° (2θ) with a constant counting time of 40 s. Structural refinement by the Rietveld method was performed using the Fullprof program.[46]

Magnetic susceptibility data were collected using an automatic susceptometer (DSM8 Manics) over the 4-300 K temperature range (applied field = 1.8 T).

Electrochemical measurements were carried out in lithium cells with the following configuration: Li/1 M $LiClO_4$ in propylene carbonate (PC)/$Li_xNi_{1-y}Mg_yO_2$ (active mass of 25 mg) with carbon black (10 wt %) as conductive agent and polyethylenetetrafluoride (PTFE) (2 wt %) as binder. Cells were assembled in an argon-filled dry box and cycled at room temperature using a home-made system monitored by a HP1000 computer operating in galvanostatic mode.[47] The electrochemical performances of the various compounds were evaluated upon cycling in the 2.7-4.15 V potential range at a C/10 rate. To permit a general comparison of all the materials, the C rate is defined as the exchange of 0.5 electrons in 1 h. Open-circuit voltage experiments were performed in the same potential range: 0.02 Li per formula unit was deintercalated (or intercalated) at each step, and the relaxation periods were interrupted as soon as the slope of the voltage *vs.* time curve was smaller than 1 mV $h^{-1}$. In addition, charges at the C/100 rate were carried out to obtain fully deintercalated $Li_xNi_{1-y}Mg_yO_2$ phases (with $y = 0.05$, 0.10, 0.15, and 0.20). In the latter case, 1 M $LiPF_6$ in a mixture of propylene carbonate (PC), dimethyl carbonate (DMC), and ethylene carbonate (EC) (1:1:3 by volume) was used as electrolyte to avoid electrolyte decomposition at potentials higher than 4.2 V.

## Results and Discussion

*Structural characterization.*—The cationic distribution, which plays a key role in the electrochemical behavior of lithium nickelates, was characterized by XRD and from magnetic measurements.

*XRD.*—Single phases isostructural to $LiNiO_2$ were obtained for $LiNi_{1-y}Mg_yO_2$ compositions with $0 \leq y \leq 0.20$. The XRD patterns of these materials are shown in Fig. 1. For all samples, the XRD lines are quite narrow, which indicates good crystallinity of the materials. Traces of $Li_2CO_3$ are observed, probably due to the presence of excess lithium in the starting mixtures. The Ni/Mg ratio was confirmed by chemical analyses, but due to the presence of a small amount of $Li_2CO_3$ in all samples, the overall set of data did not allow us to determine a true chemical formula for each magnesium-substituted phase.

For magnesium-rich compositions ($y > 0.2$), attempts to synthesize single-phase compounds, by increasing the thermal treatment temperature up to 850°C to favor chemical reaction of the starting precursors, were unsuccessful. An MgO-type phase was systematically detected by XRD. Syntheses with higher reaction temperatures were not performed because such experimental conditions are well known to favor lithium deficiency in the $Li_{1-z}Ni_{1+z}O_2$ system due to the high vapor pressure of lithium oxide at such temperatures.[7,9]

These results show that it is possible to synthesize single-phase magnesium-substituted lithium nickel oxide compounds only in a restricted composition range. Due to the difference in size and nature between nickel and magnesium ions, it is not surprising that the limit of the solid solution domain is reached rapidly. From a general point of view, the extent of the layered $LiNi_{1-y}M_yO_2$ system depends on the structural difference between the two limit phases. If an overall solid solution is thus obtained for the cobalt-substituted lithium nickelate system,[17,20,42,45] the extent of the layered structure domain is limited in all other cases: iron ($0 \leq y \leq 0.30$),[27,29,30,48] aluminum ($0 \leq y \leq 0.50$),[13,22,26] or manganese ($0 \leq y \leq 0.50$).[33-35]

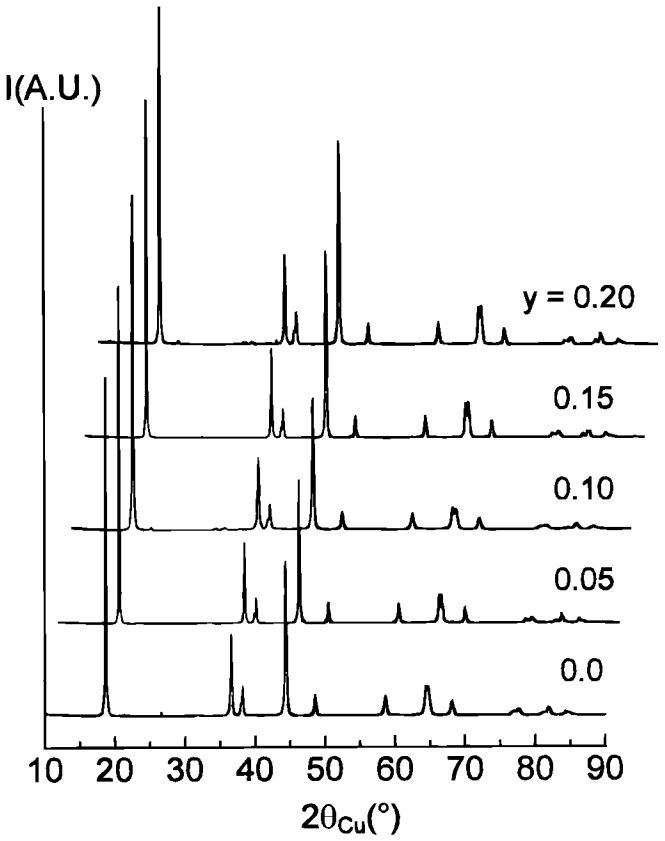


**Figure 1.** XRD patterns of magnesium-substituted $LiNi_{1-y}Mg_yO_2$ phases. The upper XRD patterns were shifted in 2θ for a better visualization.

*Rietveld refinement.*—As previously reported, refinement by the Rietveld method of the XRD patterns is a good method to characterize accurately the structure and cationic distribution for pure $Li_{1-z}Ni_{1+z}O_2$ [7,9,49-52] and substituted lithium nickelates $Li_{1-z}(Ni_{1-y}M_y)_{1+z}O_2$.[19,27,29,32,33] Indeed, the amount $z$ of extra nickel ions or extra (Ni, M) ions located in the lithium site can be determined by taking into account the strong correlation between z and the B(Li) isotropic atomic displacement parameter.[7]

In the magnesium-substituted system, if the refinement is carried out assuming a perfectly ordered α-$NaFeO_2$ type structure ($z = 0$) [space group: $R\bar{3}m$; 1 Li in the 3b site (0, 0, 0.5); (1-$y$) Ni and $y$ Mg in the 3a site (0, 0, 0)], a negative value is obtained for the B(Li) parameter. This result provides evidence for an excess of electronic density in the lithium site, as is observed in the $Li_{1-z}Ni_{1+z}O_2$ system, due to the presence of extra $Ni^{2+}$ and/or $Mg^{2+}$ ions. Because Rietveld analysis is sensitive only to the number of electrons in the various crystallographic sites of the structure, the nature of the extra ions present in the inter-slab space for lithium deficiency compensation cannot be determined directly from the Rietveld refinement. Similar agreements are thus obtained between the experimental and the calculated XRD patterns if we make the hypothesis that the residual electronic density is due either to the partial occupation of the lithium site by a single ion type ($z$ $Ni^{2+}$ or $\approx 2z$ $Mg^{2+}$) or to the undifferentiated presence of both ions ($u$ $Ni^{2+}$ + $v$ $Mg^{2+}$ with $u + v/2 \approx z$) in the 3b site. However, one can reasonably assume that, as the result of the difference in size between $Li^+$, $Ni^{2+}$, $Ni^{3+}$, and $Mg^{2+}$ ions ($r^{2+}_{Mg} = 0.72$ Å, $r^{+}_{Li} = 0.76$ Å, $r^{2+}_{Ni} = 0.69$ Å, $r^{3+}_{Ni} = 0.56$ Å),[53] the $Mg^{2+}$ ions would occupy the lithium site preferentially to the $Ni^{2+}$ ions if extra cations are required to compensate for lithium deficiency. Indeed, from a general point of view, the formation of the layered $LiMO_2$-type structure results from the size differ-

S0013-4651(99)10-069-7 CCC: $7.00 

ence between the $LiO_6$ octahedra and the $MO_6$ octahedra, so the largest cations are expected to preferentially occupy the lithium site if the Li/M ratio is smaller than 1. For instance, in the iron-substituted system, $Ni^{2+}$ and $Fe^{3+}$ ions with similar sizes ($r^{2+}_{Ni}$ = 0.69 Å, $r^{3+}_{Fe}$ = 0.645 Å) simultaneously occupy the inter-slab space,[27,29,48] whereas in the cobalt-substituted system, a very recent neutron diffraction study of lithium-deficient phases showed that only $Ni^{2+}$ ions are present in the lithium site,[54] confirming previous results deduced from steric considerations.[17,20] As is further discussed, the hypothesis of the presence of part of magnesium ions in the inter-slab space to compensate for lithium deficiency was clearly confirmed by our magnetic characterization. Therefore, Rietveld refinements were carried out considering the following cationic distribution: nickel and magnesium ions in the 3a site, lithium and a very small amount of magnesium ions in the 3b site. The occupancy parameters were refined considering that the total occupancy of each site is equal to unity and that the Mg/Ni ratio is equal to $y/(1-y)$. In the case of slightly magnesium-substituted phases, a small amount of $Ni^{2+}$ ions was also considered to be in the inter-slab space if the presence of all available magnesium ions in the 3b site only partially compensates for the lithium deficiency.

Results of Rietveld refinement for $LiNi_{0.95}Mg_{0.05}O_2$ and $LiNi_{0.80}Mg_{0.20}O_2$ are presented in detail in Tables I and II. The good agreement between the experimental and calculated patterns is given as an example for the $LiNi_{0.80}Mg_{0.20}O_2$ composition in Fig. 2. For all studied compositions, the main structural parameters and the cationic distribution are reported in Table III. The average oxidation state of nickel was calculated from each crystallographic formula (Table III). The reliability factors $R_{wp}$ and $R_B$ are good; this shows that the structural models considered describe fairly well the structure of the $LiNi_{1-y}Mg_yO_2$ compounds. For convenience, in the following discussion, the phases are still associated with their nominal chemical formula $LiNi_yMg_{1-y}O_2$, whatever the real cationic distribution.

**Table I. Refined parameters and reliability factors obtained for the structure refinement of the $LiNi_{0.95}Mg_{0.05}O_2$ phase. The standard deviations were multiplied by the Scor parameter to correct for local correlations.[46]**

| $LiNi_{0.95}Mg_{0.05}O_2$ | | | | | Constraints | |
|---|---|---|---|---|---|---|
| Space Group: $R\bar{3}m$ | | | | | $n(Li) + n(Mg_1) = 1$ | |
| $a_{hex.}$ = 2.8769(2) Å | | | | | $n(Ni) + n(Mg_2) = 1$ | |
| $c_{hex.}$ = 14.212(2) Å | | | | | $n(Ni)/[n(Mg_1) + n(Mg_2)] = 19$ | |
| | | | | | $B(Li) = B(Mg_1)$ $B(Ni) = B(Mg_2)$ | |
| Atoms | Site | Wyckoff positions | | | $B_{iso}$ (Å$^2$) | Occupancy |
| Li | 3b | 0 | 0 | 0.5 | 0.3(7) | 0.99(2) |
| $Mg_1$ | 3b | 0 | 0 | 0.5 | 0.3(7) | 0.01(2) |
| Ni | 3a | 0 | 0 | 0 | 1.03(8) | 0.96(2) |
| $Mg_2$ | 3a | 0 | 0 | 0 | 1.03(8) | 0.04(2) |
| O | 6c | 0 | 0 | 0.259(6) | 1.3(2) | 2.000 |
| Conditions of the run | | | | | | |
| → Temperature | | | | | 300 K | |
| → Angular range | | | | | $10° \le 2\theta \le 120°$ | |
| → Step scan increment (2θ) | | | | | 0.02° | |
| → Number of fitted parameters | | | | | 15 | |
| Profile parameters | | | | | | |
| Profile function: | | | | | | |
| Pseudo-Voigt $PV = \eta L + (1 - \eta)G$ | | | | | $\eta = \eta_0 + X(2\theta)$ | |
| → Eta | | | | | $\eta_0$ = 0.48(6) | |
| | | | | | $X$ = 0.006(2) | |
| → Halfwidth parameters | | | | | $U$ = −0.01(1) | |
| | | | | | $V$ = 0.05(1) | |
| | | | | | $W$ = 0.03(2) | |
| Conventional Rietveld R-factors for points with Bragg contribution | | | | | | |
| $R_{wp}$ = 12.3% $R_B$ = 2.65% | | | | | | |

**Table II. Refined parameters and reliability factors obtained for the structure refinement of the $LiNi_{0.80}Mg_{0.20}O_2$ phase. The standard deviations were multiplied by the Scor parameter to correct for local correlations.[46]**

| $LiNi_{0.80}Mg_{0.20}O_2$ | | | | | Constraints | |
|---|---|---|---|---|---|---|
| Space Group: $R\bar{3}m$ | | | | | $n(Li) + n(Mg_1) = 1$ | |
| $a_{hex.}$ = 2.8852(2) Å | | | | | $n(Ni) + n(Mg_2) = 1$ | |
| $c_{hex.}$ = 14.249(2) Å | | | | | $n(Ni)/(n(Mg_1) + n(Mg_2) = 4$ | |
| | | | | | $B(Li) = B(Mg_1)$ $B(Ni) = B(Mg_2)$ | |
| Atoms | Site | Wyckoff positions | | | $B_{iso}$ (Å$^2$) | Occupancy |
| Li | 3b | 0 | 0 | 0.5 | 0.6(4) | 0.90(2) |
| $Mg_1$ | 3b | 0 | 0 | 0.5 | 0.6(4) | 0.10(2) |
| Ni | 3a | 0 | 0 | 0 | 1.43(7) | 0.88(2) |
| $Mg_2$ | 3a | 0 | 0 | 0 | 1.43(7) | 0.12(2) |
| O | 6c | 0 | 0 | 0.2585(4) | 1.54(162) | 2.000 |
| Conditions of the run | | | | | | |
| → Temperature | | | | | 300 K | |
| → Angular range | | | | | $10° \le 2\theta \le 120°$ | |
| → Step scan increment (2θ) | | | | | 0.02° | |
| → Number of fitted parameters | | | | | 15 | |
| Profile parameters | | | | | | |
| Profile function: | | | | | | |
| Pseudo-Voigt $PV = \eta L + (1 - \eta)G$ | | | | | $\eta = \eta_0 + X(2\theta)$ | |
| → Eta | | | | | $\eta_0$ = 0.70(6) | |
| | | | | | $X$ = −0.003(1) | |
| → Halfwidth parameters | | | | | $U$ = 0.04(1) | |
| | | | | | $V$ = 0.06(1) | |
| | | | | | $W$ = 0.07(2) | |
| Conventional Rietveld R-factors for points with Bragg contribution | | | | | | |
| $R_{wp}$ = 12.0% $R_B$ = 3.35% | | | | | | |

*Magnetic behavior.*—Because the magnetic behavior of substituted lithium nickelates is expected to depend strongly on the nature of any foreign ions present in the lithium site (diamagnetic $Mg^{2+}$ ions or paramagnetic $Ni^{2+}$ ions), magnetic characterization of the $LiNi_{1-y}Mg_yO_2$ phases was carried out to confirm the partial occupation of the lithium site by $Mg^{2+}$ ions. The purpose of this study is not to make an overall magnetic characterization of these materials but only to determine their cationic distributions.

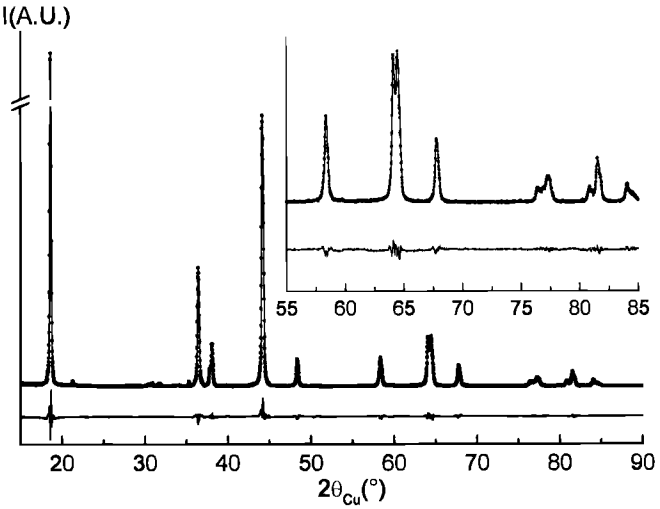


**Figure 2.** Comparison of the (-●-) experimental and (-) calculated XRD patterns for the $LiNi_{0.80}Mg_{0.20}O_2$ phase; the difference between experimental and calculated XRD pattern is also reported. The 90-120° (2θ) range is not represented to enlarge the figure.

S0013-4651(99)10-069-7 CCC: $7.00 

**Table III. Crystallographic parameters, average oxidation state for nickel ($Ni_{ox.\ state}$), cationic distribution, and reliability factors obtained from the Rietveld refinement of the XRD data of the $LiNi_{1-y}Mg_yO_2$ phases ($0 \leq y \leq 0.20$). The standard deviations were multiplied by the Scor parameter to correct for local correlations.[46]**

| $y$ in $LiNi_{1-y}Mg_yO_2$ | $a_{hex.}$ (Å) | $c_{hex.}$ (Å) | $z_{ox.}$ | $d_{Li\text{-}O}$ (Å) | $d_{Ni(Mg)O}$ (Å) | $Ni_{ox.\ state}$ | Crystallographic formula | $R_{wp}$ (%) | $R_B$ (%) |
|---|---|---|---|---|---|---|---|---|---|
| 0.0 | 2.8766(4) | 14.211(7) | 0.2596(6) | 2.122(6) | 1.964(5) | 2.96 | $[Li_{0.98}Ni^{II}_{0.02}][Ni^{III}_{0.98}Ni^{II}_{0.02}]O_2$ | 12.1 | 2.17 |
| 0.01 | 2.8759(6) | 14.205(3) | 0.2597(8) | 2.121(7) | 1.963(6) | 2.97 | $[Li_{0.98}Mg_{0.01}Ni^{II}_{0.01}][Ni^{III}_{0.98}Ni^{II}_{0.02}]O_2$ | 16.0 | 4.75 |
| 0.02 | 2.8777(3) | 14.209(2) | 0.2600(6) | 2.126(5) | 1.961(4) | 2.98 | $[Li_{0.98}Mg_{0.02}][Ni^{III}_{0.98}Ni^{II}_{0.02}]O_2$ | 11.8 | 2.85 |
| 0.05 | 2.8769(2) | 14.211(2) | 0.2595(6) | 2.121(5) | 1.964(4) | 3.03 | $[Li_{0.99}Mg_{0.01}][Ni^{III}_{0.93}Ni^{IV}_{0.03}Mg_{0.04}]O_2$ | 12.3 | 2.65 |
| 0.10 | 2.8751(2) | 14.219(2) | 0.2588(6) | 2.114(5) | 1.969(4) | 3.07 | $[Li_{0.98}Mg_{0.02}][Ni^{III}_{0.86}Ni^{IV}_{0.06}Mg_{0.08}]O_2$ | 13.2 | 2.14 |
| 0.15 | 2.8807(2) | 14.233(2) | 0.2586(5) | 2.116(4) | 1.974(4) | 3.04 | $[Li_{0.94}Mg_{0.06}][Ni^{III}_{0.86}Ni^{IV}_{0.04}Mg_{0.10}]O_2$ | 10.0 | 2.28 |
| 0.20 | 2.8852(2) | 14.249(2) | 0.2585(4) | 2.118(4) | 1.978(3) | 3.02 | $[Li_{0.90}Mg_{0.10}][Ni^{III}_{0.86}Ni^{IV}_{0.02}Mg_{0.12}]O_2$ | 12.0 | 3.35 |

As recently reported by Kanno and co-workers for a $Li_{1-z}Ni_{1+z}O_2$ composition very close to the ideal one ($z = 0.01$), a spin glass behavior is observed.[55] The presence of extra nickel ions in the lithium site strongly affects the magnetic properties of $Li_{1-z}Ni_{1+z}O_2$ compounds, which become very different from the spin glass ones. These extra nickel ions are antiferromagnetically coupled with the nickel ions located in the adjacent $NiO_2$ layers,[56] leading to the formation of ferrimagnetic clusters whose number is directly related to the amount of extra nickel ions.[7] For low $z$ values, the clusters are distributed statistically over the $LiNiO_2$ matrix and do not interact magnetically with each other. As a result, no magnetic order is observed and the thermal variation of the reciprocal susceptibility presents a Curie-Weiss behavior above a given temperature. As reported by Rougier *et al.*, magnetic property studies can then be an elegant way to quantify the amount $z$ of extra nickel ions.[7]

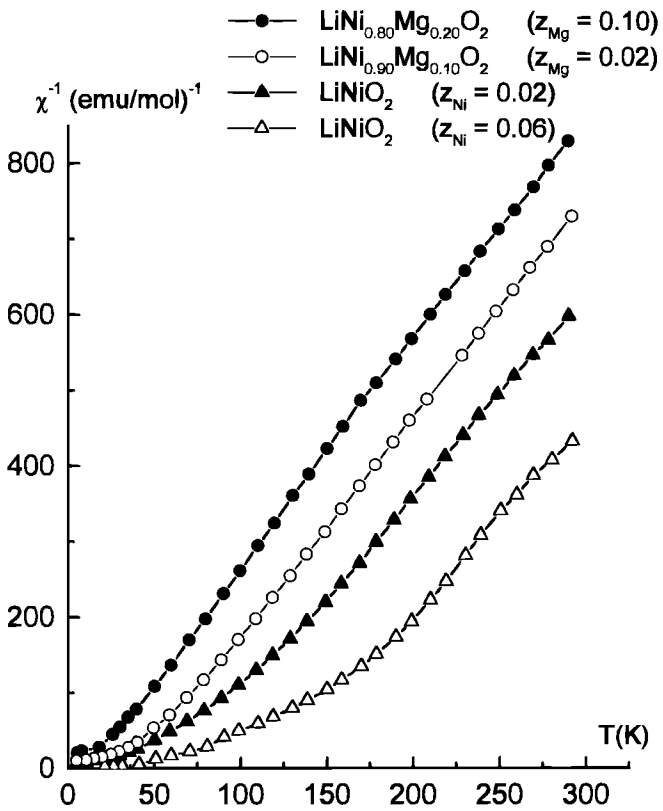


**Figure 3.** Comparison of the thermal evolution of the inverse molar magnetic susceptiblity for the $LiNi_{1-y}Mg_yO_2$ ($y = 0.10$, 0.20) and $Li_{1-z}Ni_{1+z}O_2$ phases ($z = 0.02$, 0.06) (applied field = 1.8 T). Data for $Li_{0.94}Ni_{1.06}O_2$ were taken from Ref. 7. The amount of magnesium ions ($z_{Mg}$) or nickel ions ($z_{Ni}$) located in the inter-slab space is specified in brackets.

When $z$ increases, the susceptibility becomes infinite at low temperature and the ordering temperature increases rapidly. In this study, it was shown that the effect of extra nickel ions was easily detected whatever the applied magnetic field. It was shown recently that when $z$ exceeds a threshold value $z_c \approx 0.14$, interactions between clusters become strong and percolation occurs.[57]

The thermal variations of the reciprocal molar susceptibility for the substituted $LiNi_{0.90}Mg_{0.10}O_2$ and $LiNi_{0.80}Mg_{0.20}O_2$ phases and for two lithium-deficient lithium nickelate phases are reported in Fig. 3. The data related to the $Li_{1-z}Ni_{1+z}O_2$ phase ($z = 0.06$) have been taken from previously reported results.[7] The observed difference between the magnetic curves of the $Li_{0.98}Ni_{1.02}O_2$ and $Li_{0.94}Ni_{1.06}O_2$ compounds clearly illustrates the presence of ferrimagnetic clusters in the most lithium-deficient material, as previously discussed.[58] The shape of the susceptibility curve of $Li_{0.98}Ni_{1.02}O_2$ is comparable to that reported by Kanno *et al.* for the $Li_{0.99}Ni_{1.01}O_2$ composition.[55] Moreover, some of these authors showed, in a previous paper for the $Li_{0.95}Ni_{1.05}O_2$ composition, behavior similar to that observed for $Li_{0.94}Ni_{1.06}O_2$. The presence of ferrimagnetic domains in the latter material was also evidenced by the existence of a hysteresis loop which is not detected for the $Li_{0.98}Ni_{1.02}O_2$ composition.[59]

However, Fig. 3 also emphasizes different magnetic behaviors for the magnesium-substituted and the nonsubstituted materials. Indeed, for $LiNi_{0.90}Mg_{0.10}O_2$ and $LiNi_{0.80}Mg_{0.20}O_2$, the variation of the reciprocal susceptibility is similar to that reported for nearly stoichiometric $LiNiO_2$. It is characteristic of a Curie-Weiss paramagnetic-type behavior above 70 K. Note that for $LiNi_{0.80}Mg_{0.20}O_2$ there is an abnormality at about 175 K in the susceptibility curve. In comparison to the spin glass behavior of $LiNiO_2$, the presence of a part of the diamagnetic $Mg^{2+}$ ions in the nickel site must break the in-plane tension and therefore induce a more complicated magnetic behavior. A comparison of the experimental Curie constants (calculated for above 175 K) with the theoretical ones in Table IV confirms the chemical formula deduced from the Rietveld refinement. The difference observed between the shapes of the magnetic curves of the magnesium-substituted materials and that of $Li_{0.98}Ni_{1.02}O_2$ shows that the amount of ferrimagnetic clusters is negligible in the two substituted compounds. As a significant amount of $Mg^{2+}$ (or $Ni^{2+}$) ions

**Table IV. Variation with $y$ of the Curie constants of the $LiNi_{1-y}Mg_yO_2$ phases ($y = 0.0$, 0.10, and 0.20). The experimental values were calculated in the 175-300 K temperature range.**

| $y$ in $LiNi_{1-y}Mg_yO_2$ | Formula deduced from the Rietveld refinement | Curie constant $C_{theor.}$ | Curie constant $C_{exp.}$ |
|---|---|---|---|
| 0.0 | $[Li_{0.98}Ni^{II}_{0.02}][Ni^{III}_{0.98}Ni^{II}_{0.02}]O_2$ | 0.41 | 0.37 |
| 0.10 | $[Li_{0.98}Mg_{0.02}][Ni^{III}_{0.86}Ni^{IV}_{0.06}Mg_{0.08}]O_2$ | 0.32 | 0.34 |
| 0.20 | $[Li_{0.90}Mg_{0.10}][Ni^{III}_{0.86}Ni^{IV}_{0.02}Mg_{0.12}]O_2$ | 0.32 | 0.35 |

S0013-4651(99)10-069-7 CCC: $7.00 

was detected by Rietveld refinement for $LiNi_{0.80}Mg_{0.20}O_2$, the paramagnetic behavior at low temperature shows that there are no paramagnetic $Ni^{2+}$ ions in the lithium site and clearly confirms that only diamagnetic $Mg^{2+}$ ions are located in excess in the inter-slab space. In the hypothesis of $Ni^{2+}$ in the lithium site, the susceptibility curve would be similar to that for $Li_{0.94}Ni_{1.06}O_2$, which is not the case.

These results show that our magnetic-properties study is an effective way to confirm that for lithium-deficient phases, the divalent ions which are present in the lithium site to ensure charge compensation are preferentially $Mg^{2+}$ ions instead of $Ni^{2+}$ ions. Also, this technique was recently employed to prove in the same way that $Ni^{2+}$ ions are located in the inter-slab space for aluminum-substituted nickelates.[60]

*Cell parameters and cationic distribution.*—The evolution with $y$ of the structural parameters, average oxidation state of nickel ($Ni_{ox.\ state}$) and amount of extra cations present in the lithium site ($z$) is given in Fig. 4 for the $LiNi_{1-y}Mg_yO_2$ phases.

Two main domains must be considered depending on the $y$ values. For the small values ($y \leq 0.10$), the total amount of extra cations ($Mg^{2+}$ and/or $Ni^{2+}$) located in the lithium site is nearly constant (Fig. 4e). Therefore, there is no significant change in the cell parameters (Fig. 4a-c). For the highest magnesium content, the increasing amount of $Mg^{2+}$ ions situated either in the slab or in the inter-slab space leads to an increase of both $a_{hex.}$ and $c_{hex.}$ parameters (Fig. 4a-b).

In the previous section, we have assumed from size considerations and shown from magnetic measurements that when extra cations are required in the lithium site to compensate for lithium deficiency, these ions are preferentially $Mg^{2+}$ rather than $Ni^{2+}$.

For slightly magnesium-substituted lithium nickelates $LiNi_{1-y}Mg_yO_2$ ($0 < y \leq 0.02$), the lithium deficiency required the presence of all $Mg^{2+}$ ions in the inter-slab space. For small $y$ values ($y = 0.01$), there are not enough $Mg^{2+}$ ions to compensate for lithium deficiency, therefore $Ni^{2+}$ ions are also required. For $y = 0.02$, there are only $Mg^{2+}$ ions in the lithium site. Such cationic distributions imply the presence of $Ni^{2+}$ ions within the slab for charge compensation. Therefore, the average oxidation state of nickel in the materials remains smaller than 3+ (Fig. 4d).

For the magnesium-rich materials ($y = 0.05$, 0.10), only a small amount of $Mg^{2+}$ ions is present in the inter-slab space. The slab is therefore simultaneously occupied by $Mg^{2+}$, $Ni^{3+}$, and a small amount of $Ni^{4+}$ ions for charge compensation. The presence of $Ni^{4+}$ ions induces an average oxidation state higher than 3+ for nickel (Fig. 4d).

For the $LiNi_{0.85}Mg_{0.15}O_2$ and $LiNi_{0.80}Mg_{0.20}O_2$ compositions, a surprisingly large amount of $Mg^{2+}$ ions is located in the lithium site, which induces a decrease in the mean oxidation state for nickel (Fig. 4d). If for such substitution rates the amount of extra magnesium ions remained close to 2%, the charge compensation would require an increasing amount of $Ni^{4+}$ ions in the slab but the large size of $Mg^{2+}$ destabilizes the tetravalent nickel ions. Therefore, the amount of $Ni^{4+}$ ions in the slab decreases when $y$ increases and an increasing amount of $Mg^{2+}$ ions is required in the inter-slab space to ensure electroneutrality (Fig. 4d-e). In other words, the cationic distribution for the $LiNi_{0.85}Mg_{0.15}O_2$ and $LiNi_{0.80}Mg_{0.20}O_2$ materials can be related to synthesis conditions. If there was a small departure from stoichiometry (with a very small amount of $Mg^{2+}$ ions in the lithium site), a large $Ni^{4+}/Ni^{3+}$ ratio would be required. However, as previously suggested,[60] during synthesis the oxidizing power of the medium is not expected to be high enough to obtain such large amounts of tetravalent nickel ions, and therefore a significant amount of magnesium ions are situated in the lithium site in order to reduce the average oxidation state of nickel in the material.

*Electrochemical behavior.*—A general electrochemical study was carried out to determine the effect of magnesium substitution on the electrochemical behavior of the $Li_xNi_{1-y}Mg_yO_2$ materials ($0 \leq y \leq 0.20$).

Figure 5 shows the variation of cell voltage *vs.* lithium amount during the first ten charge-discharge cycles (at the C/10 rate) obtained for various magnesium-substituted phases ($y = 0.0$, 0.01, 0.02, 0.05, 0.10, 0.15). The average reversible capacity calculated over 10 cycles is also reported in this figure. In all cases, the lithium deintercalation-intercalation process is highly reversible with small polarization, which demonstrates that whatever the magnesium amount, the mate-

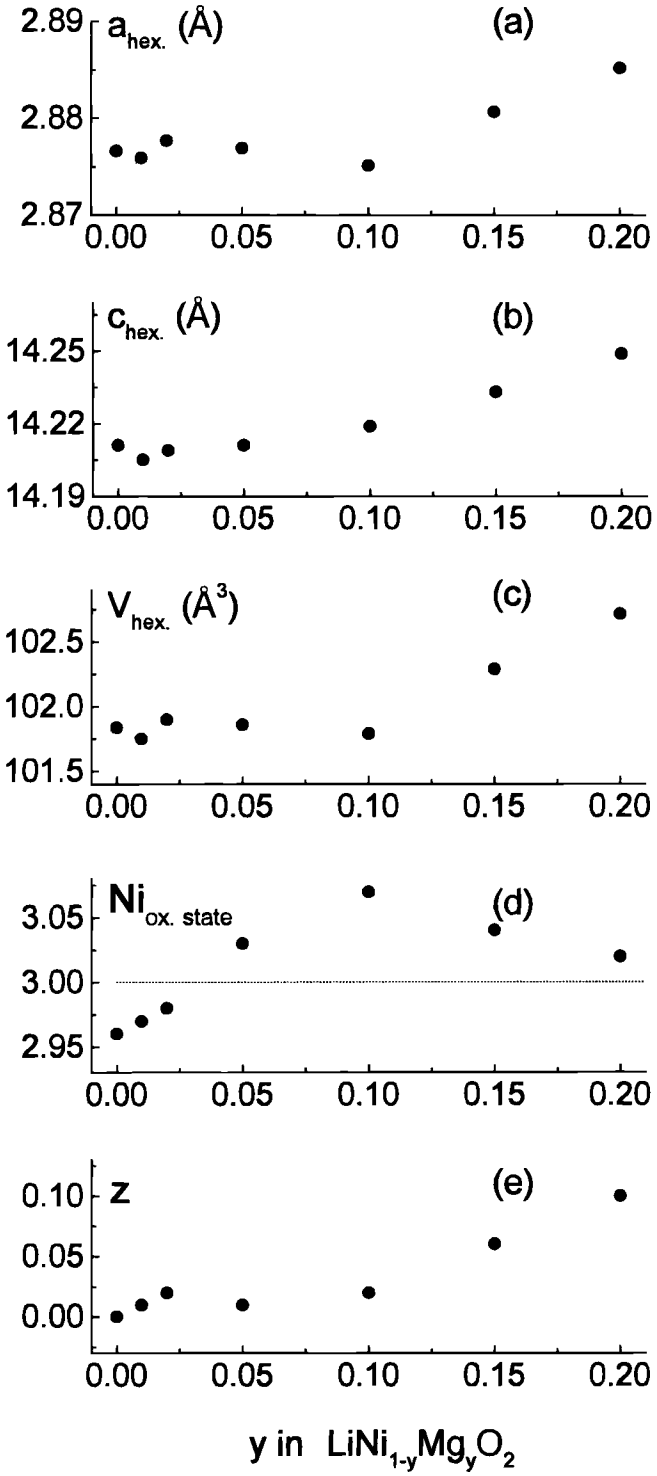


**Figure 4.** Variation *vs.* $y$ of the $a_{hex.}$ and $c_{hex.}$ cell parameters, of the unit cell volume $V_{hex.}$, of the average oxidation state of nickel ions ($Ni_{ox.\ state}$) (deduced from structural data) and of the amount of extra cations in the lithium site ($z$) for the $LiNi_{1-y}Mg_yO_2$ phases ($0 \leq y \leq 0.20$).

S0013-4651(99)10-069-7 CCC: $7.00 © The Electrochemical Society, Inc.

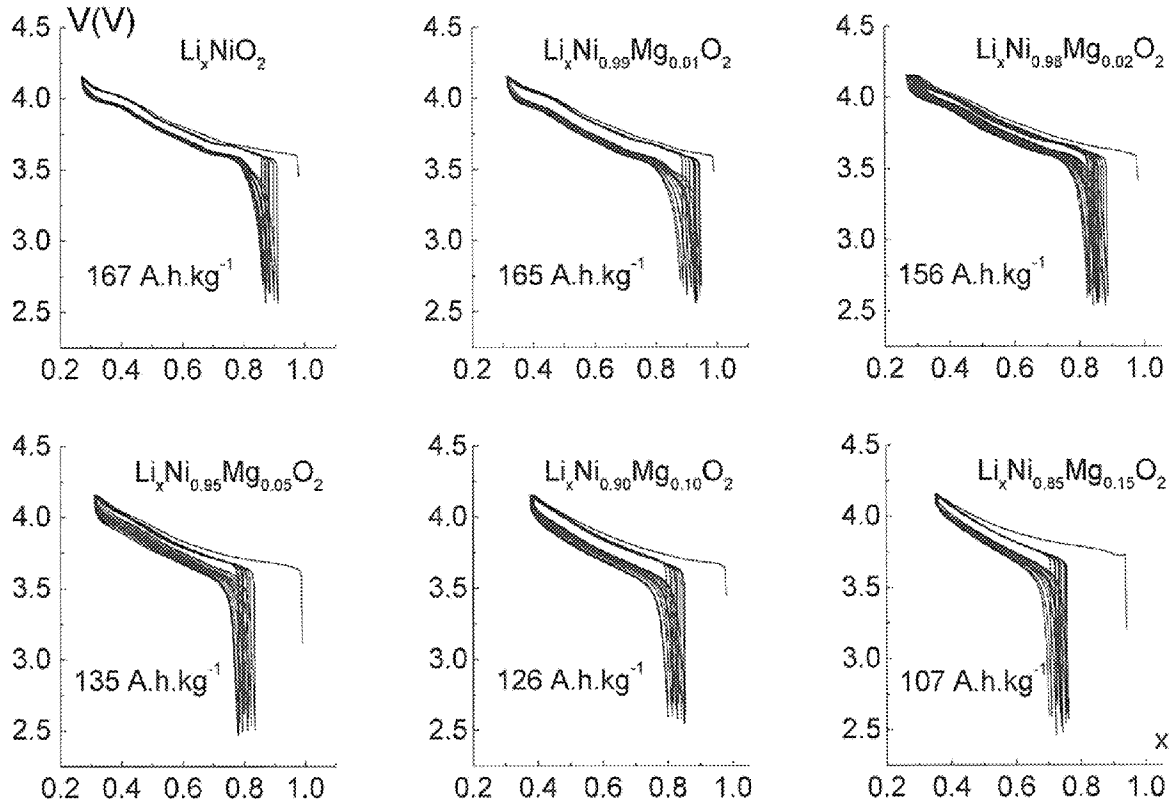


**Figure 5.** Variation of the cell voltage *vs.* composition for the first ten galvanostatic charge/discharge cycles of Li//$LiNi_{1-y}Mg_yO_2$ cells ($y$ = 0.0, 0.01, 0.02, 0.05, 0.10, 0.15) at the C/10 rate. The average reversible specific capacity over 10 cycles is specified for each composition.

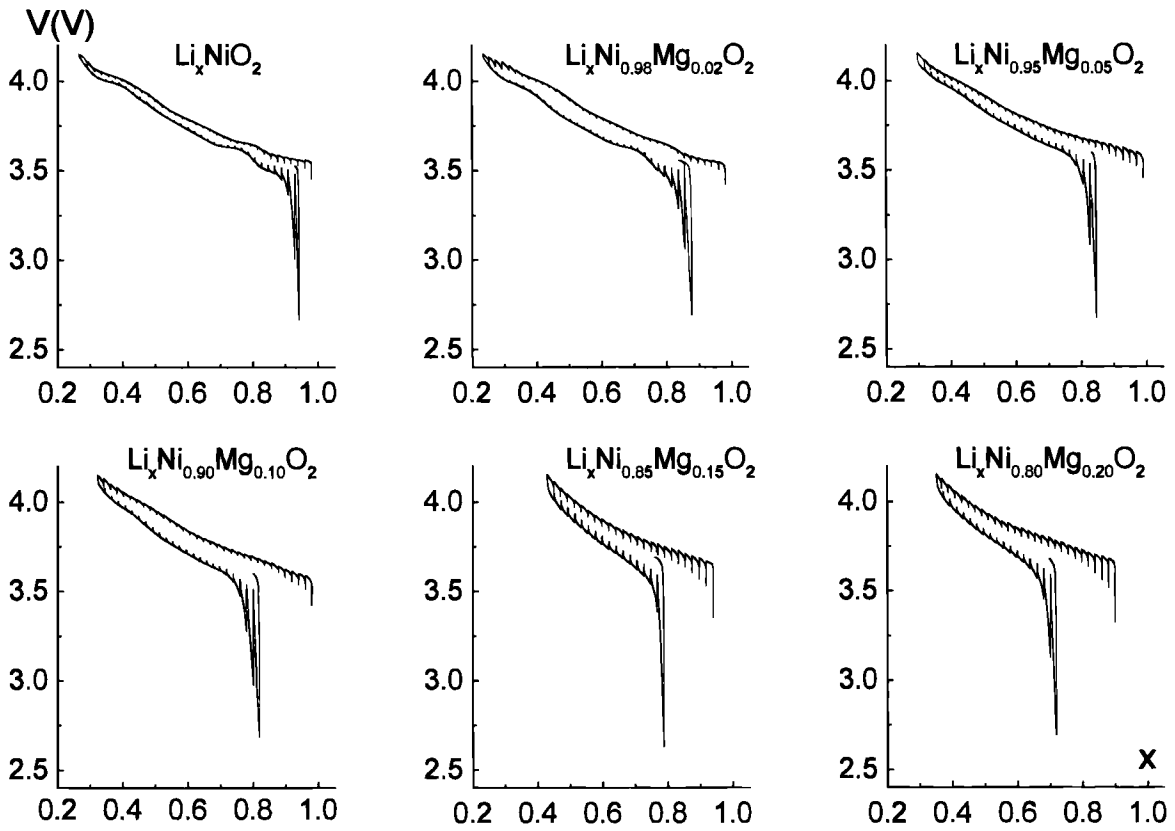


**Figure 6.** Variation of the cell voltage *vs.* composition during the first open-circuit voltage, charge/discharge of Li//$LiNi_{1-y}Mg_yO_2$ cells ($y$ = 0, 0.02, 0.05, 0.10, 0.15, 0.20). Each 100 min long step corresponds to the intercalation-deintercalation of 0.02 Li; the relaxation period was interrupted when the slope of the voltage curve was smaller than 1 mV/h.

S0013-4651(99)10-069-7 CCC: $7.00 

rial exhibits good cycling behavior. Furthermore, good reversible capacities, higher than 130 Ah $kg^{-1}$, are obtained for small $y$ values, and the capacities tend to decrease when $y$ increases. Indeed, as magnesium ions remain in the divalent state, the $Li_xNi_{1-y}Mg_yO_2$ phases are electron-donor limited. Taking the cationic distribution of the materials into account (Table III), the number of electrons which can be exchanged upon cycling decreases with the decrease of the number of $Ni^{3+}$ ions present in the pristine material, and as a result the theoretical reversible capacity decreases with y.

In order to approach thermodynamic equilibrium, the $Li//Li_xNi_{1-y}Mg_yO_2$ cells ($y$ = 0.0, 0.02, 0.05, 0.10, 0.15, 0.20) were cycled at a low rate with alternate periods of relaxation (Fig. 6). The electrochemical curves exhibit a continuous trend with the amount of magnesium. In most of the intercalation-deintercalation range, the cell polarization (given by the height of vertical lines on the $V = f(x)$ plot) is very small, which suggests rapid lithium diffusion kinetics. The polarization tends to increase slightly for $y$ = 0.15 and $y$ = 0.20, in relation to the increase of magnesium amount in the inter-slab space. At the end of discharge, the cell polarization increases sharply due to decreasing ionic conductivity when most of the inter-slab sites are occupied. A surprisingly large loss of reversibility is observed at the end of the first cycle for the magnesium-substituted materials and appears to be in contradiction with the quasi-two-dimensional structure of the $LiNi_{0.95}Mg_{0.05}O_2$ and $LiNi_{0.90}Mg_{0.10}O_2$ materials (almost no foreign cations are present in the inter-slab space). A preliminary structural study of the $Li_xNi_{1-y}Mg_yO_2$ phases showed that irreversible magnesium migration from the slab to the inter-slab space occurs during the first charge, leading to a significant irreversible capacity at the first cycle. These results will be published in a forthcoming paper.

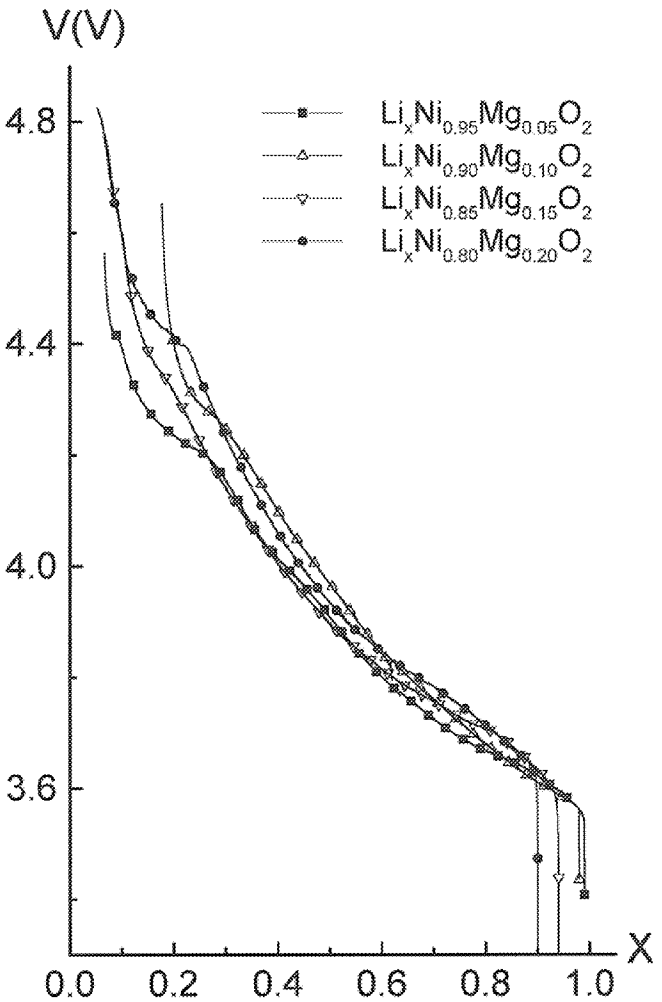


**Figure 7.** Variation of the cell voltage *vs.* composition during the first overall charge of the $Li//LiNi_{1-y}Mg_yO_2$ cells ($y$ = 0.05, 0.10, 0.15, 0.20).

The voltage plateaus characteristic of the phase transitions observed during the lithium deintercalation process for quasi-stoichiometric $Li_{1-z}Ni_{1+z}O_2$ phases ($z < 0.05$),[61-64] are clearly visible on the electrochemical curve obtained for the $LiNi_{0.98}Mg_{0.02}O_2$ material. For $y \geq 0.05$, the potential-composition curve becomes almost monotonic; which suggests the existence of a solid-solution domain over the entire intercalation-deintercalation composition range. It thus appears that substitution of 5% Mg for Ni is high enough to suppress all phase transitions observed for the $Li_xNiO_2$ system which are associated with lithium/vacancy orderings in the inter-slab space.[15,64] In the case of the $LiNi_{1-y}Co_yO_2$ system, the amount of substitution required to suppress the phase transition upon lithium deintercalation is significantly higher ($y \geq 0.20$ [18,65]). In the magnesium-substituted system, one can assume that the magnesium migration previously mentioned tends to destabilize the ordered phases.

The overall charge curves (up to a high potential) obtained for the $LiNi_{1-y}Mg_yO_2$ materials ($y$ = 0.05, 0.10, 0.15, 0.20) are reported in Fig. 7. The maximum amount of lithium ions which can be effectively extracted during a full charge is related strongly to the nickel oxidation state in the starting phase. Indeed, 0.8 lithium ion ($= \Delta x_{exp.}$) can be experimentally extracted from the $LiNi_{0.90}Mg_{0.10}O_2$ phase. This value is very close to the theoretical one ($\Delta x_{theor.} = 0.86$) which results from the oxidation of the 0.86 $Ni^{3+}$ ion present in the slab of the pristine material. The same observation can be made for the other materials, as is illustrated in Table V by the small difference observed between the theoretical ($\Delta x_{theor.}$) and experimental ($\Delta x_{exp.}$) deintercalated lithium amounts. These results are in good agreement with the cationic distribution deduced from Rietveld refinement of the XRD patterns. They show that, at least in the considered potential range, only nickel ions are involved in the redox process.

This electrochemical study allowed us to demonstrate the good reversible cycling behavior of magnesium-substituted lithium nickel oxides. It is well known that in the $Li_{1-z}Ni_{1+z}O_2$ system, the amount $z$ of extra nickel ions strongly affects the electrochemical properties of the materials as it entails an increase of both polarization and irreversible capacity at the first cycle. Even if the $LiNi_{0.85}Mg_{0.15}O_2$ material does not exhibit high reversible capacity, it presents good cycling stability. This difference can be attributed to the difference in nature of the foreign ions located in the lithium site for the two systems. As previously reported, in the $Li_xNiO_2$ system the dramatic deterioration of electrochemical performances is strongly related to the change in oxidation state of the extra nickel ions, which induces local collapses of the structure and hinders not only lithium diffusion in the inter-slab space but also lithium reintercalation in the six sites around each extra nickel ion (Fig. 8a).[10,11] In the $Li_xNi_{1-y}Mg_yO_2$ system, the magnesium ions, with a size very close to that of lithium, remain in the divalent state during cell charge. Therefore, their

**Table V. Comparison of the experimental $\Delta x_{exp.}$ and theoretical $\Delta x_{theor.}$ amounts of lithium ions which can be deintercalated during an overall charge of the $Li//LiNi_{1-y}Mg_yO_2$ cells ($0.05 \leq y \leq 0.20$). The $\Delta x_{exp.}$ values were determined from the electrochemical experiments reported in Fig. 7. The $\Delta x_{theor.}$ values were calculated from the formulas deduced from the Rietveld refinement results.**

| $y$ in $LiNi_{1-y}Mg_yO_2$ | Formula deduced from the Rietveld refinement | Lithium amount $\Delta x_{theor.}$ | Lithium amount $\Delta x_{exp.}$ |
|---|---|---|---|
| 0.05 | $[Li_{0.99}Mg_{0.01}][Ni^{III}_{0.93}Ni^{IV}_{0.03}Mg_{0.04}]O_2$ | 0.93 | 0.92 |
| 0.10 | $[Li_{0.98}Mg_{0.02}][Ni^{III}_{0.86}Ni^{IV}_{0.06}Mg_{0.08}]O_2$ | 0.86 | 0.80 |
| 0.15 | $[Li_{0.98}Mg_{0.06}][Ni^{III}_{0.86}Ni^{IV}_{0.04}Mg_{0.10}]O_2$ | 0.86 | 0.87 |
| 0.20 | $[Li_{0.90}Mg_{0.10}][Ni^{III}_{0.86}Ni^{IV}_{0.02}Mg_{0.12}]O_2$ | 0.86 | 0.85 |

S0013-4651(99)10-069-7 CCC: $7.00 

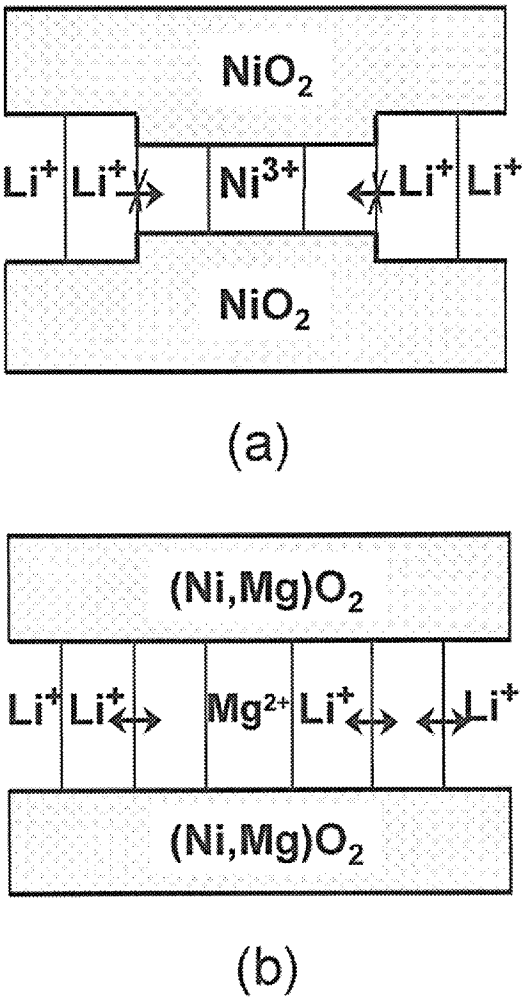


**Figure 8.** Schematic representation of the inter-slab space: (a) in the $Li_xNi_{1+z}O_2$ system, the oxidation of the $Ni^{2+}$ ions during the first electrochemical cycle induces a local collapse of the inter-slab space which makes difficult lithium diffusion and re-intercalation; (b) the $Li_xNi_{1-y}Mg_yO_2$ system, the electrochemically inactive $Mg^{2+}$ ions do not hinder lithium diffusion since their size is very close to $Li^+$.

presence in the inter-slab space does not strongly affect lithium reintercalation because no shrinkage of the structure appears upon cycling (Fig. 8b). This result explains why the magnesium-substituted phases have good cycling properties.

## Conclusions

Steric and electrostatic considerations imply that the quasi-two-dimensional structure of $LiNi_{1-y}Mg_yO_2$ materials is characterized by the presence of $Mg^{2+}$ ions in the inter-slab space for lithium-deficiency compensation. The inactive character of this substituting cation from the electrochemical point of view and its size similarity to lithium explain the good reversible capacity of these magnesium-substituted lithium nickelates: the presence of magnesium ions in the lithium site prevents any local collapse of the inter-slab space during the deintercalation process.

## Acknowledgments

The authors thank M. Ménétrier for fruitful discussions, B. Delatouche, and L. Tarascon for technical assistance, and SAFT, CNES, RÈgion Aquitaine, ANRT, and CEE (contract CT960064) for financial support.

*The Institut de Chimie de la Matière Condensée de Bordeaux assisted in meeting the publication costs of this article.*

## References

1. M. G. S. R. Thomas, W. I. F. David, J. B. Goodenough, and P. Groves, *Mater. Res. Bull.*, **20**, 1137 (1985).
2. M. Broussely, F. Perton, J. Labat, R. J. Staniewicz, and A. Romero, *J. Power Sources*, **43-44**, 209 (1993).
3. M. Broussely, F. Perton, Ph. Biensan, J. M. Bodet, J. Labat, A. Lecerf, C. Delmas, A. Rougier, and J. P. Pérès, *J. Power Sources*, **54**, 109 (1995).
4. J. R. Dahn, U. von Sacken, M. W. Juzkow, and H. Al-Janaby, *J. Electrochem. Soc.*, **138**, 2207 (1991).
5. T. Ohzuku and A. Ueda, *Solid State Ionics*, **69**, 201 (1994).
6. L. D. Dyer, B. S. Borie, and G. P. Smith, *J. Am. Chem. Soc.*, 1499 (1954).
7. A. Rougier, P. Gravereau, and C. Delmas, *J. Electrochem. Soc.*, **143**, 1168 (1996).
8. H. Arai, S. Okada, H. Ohtsuka, M. Ichimura, and J. Yamaki, *Solid State Ionics*, **80**, 261 (1995).
9. R. Kanno, H. Kubo, Y. Kawamoto, T. Kamiyama, F. Izumi, Y. Takeda, and M. Takano, *J. Solid State Chem.*, **110**, 216 (1994).
10. J. P. Pérès, C. Delmas, A. Rougier, M. Broussely, F. Perton, Ph. Biensan, and P. Willmann, *J. Phys. Chem. Solids*, **57**, 1057 (1996).
11. C. Delmas, J. P. Pérès, A. Rougier, A. Demourgues, F. Weill, A. Chadwick, M. Broussely, F. Perton, Ph. Biensan, and P. Willmann, *J. Power Sources*, **68**, 120 (1997).
12. J. R. Dahn, E. W. Fuller, M. Obrovac, and U. von Sacken, *Solid State Ionics*, **69**, 265 (1994).
13. T. Ohzuku, A. Ueda, and M. Kouguchi, *J. Electrochem. Soc.*, **142**, 4033 (1995).
14. H. Arai, S. Okada, Y. Sakurai, and J. Yamaki, *Solid State Ionics*, **109**, 295 (1998).
15. J. P. Pérès, Thesis, University of Bordeaux I (1996).
16. C. Delmas, J. P. Pérès, C. Louchet, F. Weill, M. Broussely, F. Perton, Ph. Biensan, A. de Guibert, and P. Willmann, in Extended Abstracts of the 9th International Meeting on Lithium Batteries (1998).
17. C. Delmas and I. Saadoune, *Solid State Ionics*, **53-56**, 370 (1992).
18. C. Delmas, I. Saadoune, and A. Rougier, *J. Power Sources*, **43-44**, 595 (1993).
19. A. Rougier, I. Saadoune, P. Gravereau, P. Willmann, and C. Delmas, *Solid State Ionics*, **90**, 83 (1996).
20. E. Zhecheva and R. Stoyanova, *Solid State Ionics*, **66**, 143 (1993).
21. A. Ueda and T. Ohzuku, *J. Electrochem. Soc.*, **141**, 2010 (1994).
22. A. Rougier, Thesis, University of Bordeaux I (1995).
23. G. X. Wang, S. Zhong, D. H. Bradhurst, S. X. Dou, and H. K. Liu, *Solid State Ionics*, **116**, 271 (1999).
24. T. Ohzuku, T. Yanagawa, M. Kouguchi, and A. Ueda, *J. Power Sources*, **68**, 131 (1997).
25. Q. Zhong and U. von Sacken, *J. Power Sources*, **54**, 221 (1995).
26. T. Ohzuku and K. Nakura, *Denki Kagaku oyobi Kogyo Butsuri Kagaku*, **66**, 1209 (1998).
27. J. N. Reimers, E. Rossen, C. D. Jones, and J. R. Dahn, *Solid State Ionics*, **61**, 335 (1993).
28. R. Kanno, T. Shirane, Y. Inaba, and Y. Kawamoto, *J. Power Sources*, **68**, 145 (1997).
29. G. Prado, E. Suard, L. Fournès, and C. Delmas, *J. Mater. Chem.*, Submitted.
30. G. Prado, A. Rougier, L. Fournès, P. Willmann, and C. Delmas, *J. Electrochem. Soc.*, To be published.
31. S. H. Chang, S. Kang, S. Song, J. Yoon, and J. Choy, *Solid State Ionics*, **86-88**, 171 (1996).
32. H. Arai, S. Okada, Y. Sakurai, and J. Yamaki, *J. Electrochem. Soc.*, **144**, 3117 (1997).
33. E. Rossen, C. D. W. Jones, and J. R. Dahn, *Solid State Ionics*, **57**, 311 (1992).
34. D. Caurant, N. Baffier, V. Bianchi, G. Grégoire, and S. Bach, *J. Mater. Chem.*, **6**, 1149 (1996).
35. M. E. Spahr, P. Novak, B. Schnyder, O. Haas, and R. Nesper, *J. Electrochem. Soc.*, **145**, 1113 (1998).
36. Y. Nitta, K. Okamura, K. Haraguchi, S. Kobayashi, and A. Ohta, *J. Power Sources*, **54**, 511 (1995).
37. M. Yoshio, Y. Todorov, K. Yamato, H. Noguchi, J. I. Itoh, M. Okada, and T. Mouri, *J. Power Sources*, **74**, 46 (1998).
38. Y. Nishida, K. Nakane, and T. Satoh, *J. Power Sources*, **68**, 561 (1997).
39. G. A. Nazri, A. Rougier, and C. Julien, in Paper A-12, Extended Abstracts of the 12th International Conference on Solid State Ionics (1999).
40. Y. Gao, M. V. Yakovleva, and W. B. Ebner, *Electrochem. Solid-State Lett.*, **1**, 117 (1998).
41. A. Yu, G. V. Subba Rao, and B. V. R. Chowdari, in Paper A-18, Extended Abstracts of the 12th International conference on Solid State Ionics (1999).
42. I. Saadoune and C. Delmas, *J. Mater. Chem.*, **6**, 193 (1996).
43. H. Tukamoto and A. R. West, *J. Electrochem. Soc.*, **144**, 3164 (1997).
44. F. Perton, Ph. Biensan, J. P. Pérès, and M. Broussely, Private communication,
45. D. Caurant, N. Baffier, B. Garcia, and J. P. Pereira-Ramos, *Solid State Ionics*, **91**, 45 (1996).
46. J. Rodriguez-Carvajal, in *Satellite Meeting on Powder Diffraction of the XV Congress of the IUCr*, p. 127 (1990).
47. A. Mendiboure and C. Delmas, *Comput. Chem.*, **11**, 153 (1987).
48. C. Delmas, G. Prado, A. Rougier, E. Suard, and L. Fournès, *Solid State Ionics*, In press.
49. A. Hirano, R. Kanno, Y. Kawamoto, Y. Takeda, K. Yamaura, M. Takano, K. Ohyama, M. Ohashi, and Y. Yamaguchi, *Solid State Ionics*, **78**, 123 (1995).
50. W. Li, J. N. Reimers, and J. R. Dahn, *Phys. Rev. B*, **46**, 3236 (1992).
51. J. N. Reimers, J. R. Dahn, J. E. Greedan, C. V. Stager, G. Liu, I. Davidson, and U. von Sacken, *J. Solid State Chem.*, **102**, 542 (1993).

S0013-4651(99)10-069-7 CCC: $7.00 

52. J. Morales, C. Pérez-Vicente, and J. L. Tirado, *Mater. Res. Bull.*, **25**, 623 (1990).
53. R. D. Shannon and C. T. Prewitt, *Acta Crystallogr.*, **B25**, 925 (1969).
54. K. K. Lee and K. B. Kim, *J. Electrochem. Soc.*, **147**, 1709 (2000).
55. T. Shirakami, M. Takematsu, A. Hirano, R. Kanno, K. Yamaura, M. Takano, and T. Atake, *Mater. Sc. Eng., B*, **54**, 70 (1998).
56. J. B. Goodenough, D. G. Wickham, and W. J. Croft, *J. Appl. Phys.*, **29**, 382 (1958).
57. D. Mertz, Y. Ksari, F. Celestini, J. M. Debierre, A. Stepanov, and C. Delmas, *Phys. Rev. B*, Submitted.
58. A. Rougier, C. Delmas, and G. Chouteau, *J. Phys. Chem. Solids*, **57**, 1101 (1996).
59. A. L. Barra, G. Chouteau, A. Stepanov, A. Rougier, and C. Delmas, *Eur. Phys. J. B*, **7**, 551 (1999).
60. C. Delmas, M. Ménétrier, L. Croguennec, I. Saadoune, A. Rougier, C. Pouillerie, G. Prado, M. Grüne, and L. Fournès, *Electrochim. Acta*, **45**, 243 (1999).
61. T. Ohzuku, A. Ueda, and M. Nagayama, *J. Electrochem. Soc.*, **140**, 1862 (1993).
62. W. Li, J. N. Reimers, and J. R. Dahn, *Solid State Ionics*, **67**, 123 (1993).
63. H. Arai, S. Okada, Y. Sakurai, and J. I. Yamaki, *Solid State Ionics*, **95**, 275 (1997).
64. J. P. Pérès, F. Weill, and C. Delmas, *Solid State Ionics*, **116**, 19 (1999).
65. I. Saadoune and C. Delmas, *J. Solid State Chem.*, **136**, 8 (1998).